PROCEEDINGS OF SPIE

X-Ray and Neutron Capillary Optics II

Muradin A. Kumakhov
Editor

22–26 September 2004
Zvenigorod, Russia

Organized by
Institute for Roentgen Optics (Russia)

Co-organized and sponsored by
SPIE—The International Society for Optical Engineering
SPIE Russia Chapter
Unisantis S.A. (Switzerland)

Volume 5943

The International Society for Optical Engineering

X-Ray Optical Projection Microscope Based of Polycapillary Kumakhov Optics

A.G. Touriyanski*[a], O.A. Matveeva[b], N.Yu. Narimanova[a], I.V. Pirshin[a]

[a]P.N. Lebedev Physical Institute, Russian Academy of Sciences, Leninskii pr. 53, Moscow, 119991 Russia,

[b]Institute for Roentgen Optics, 1-st Volokolamsky proezd, 10, Moscow, 123060, Russia

ABSTRACT

The X-ray projection microscope with the use of polycapillary optics is described. The focusing Kumakhov lens with a focus size of 150 μm and an energy-dispersive Si-detector allow local analysis of chemical elements concentrations and distributuions. The same lens can be used for local radiation procession with a dose rate up to 10 Gy/s. Digital projections are recorded by the 1300x1030 detecting array with a pixel size of 6.7 μm. The radiation spectrum can be strongly modulated by changing X-ray source voltage, rotation the filter cassette, and by placing in the incident beam the polycapillary half-lens. Conditions for enhancing image contrast by the digital subtraction of X-ray projections registered at different spectrum distributions in the energy range of 5–25 keV are considered. It is shown that when an object is irradiated by polychromatic radiation, the use of a Ni filter and a $NiCl_2$ contrast solution provides results that were previously obtained by subtracting images with monochromatic spectral lines near the *K*- jump of absorption in the contrast media. X-ray fluorescence spectra and contrast enhanced images of biological objects are presented.

Key words: X-ray microscopy, image subtraction, Kumakhov polycapillary optics.

1. INTRODUCTION

Investigation of internal structure of biological objects usually brings up three basic tusks: a – reliable determination low-contrast details, b - non-destructive detecting of chemical elements in a small region of interest, and c – treatment of biological samples. An efficient method for solving the first problem is the contrast enhancement of the object's internal structure using a substance with a linear absorption coefficient μ that significantly differs from the corresponding parameter of the environment. This technique is widely used in medicine, where contrasting is usually provided with the help of compounds of heavy elements with atomic numbers $Z > 50$: I, Ba, Ta, and Xe .[1-4] In some cases, air or other gases can be pumped into the cavity.[1,2] When the volume of the object under study or an adjacent region between organs is filled with a gas, the increase in their volumes additionally contributes to the improvement of the contrast.

Combining the methods of contrasting and subtracting images, which were obtained, for example, before and after the introduction of a contrast substance[5], allows to obtain more sensitive diagnostic technique. This makes it possible to largely reduce the effect of the superposition of images of various internal organs and to selectively distinguish structures filled with contrast media. The selective discrimination of the structural details is especially efficient when narrow spectral bands are used, which are positioned on both sides of the *K*-jump in the photoabsorption spectrum of the contrasting element.[6,7] When two detecting systems are used, the projection schemes also allow dynamic subtraction images to be obtained. The procedure of the dynamic subtraction of images has become technically efficient after putting into practice digital methods for data registration, image-field discretization describing the field in the form of a matrix. Each element of this matrix characterizes a local value of the radiation flux density transmitted through the object. However, the methods of recording subtraction images with the selection of predetermined spectral bands are not widely practiced. This is due to the necessity of using synchrotron sources whose technical parameters exclude their application in clinical conditions for the time being.[8] This work shows that the methods of deep spectrum modulation provide sharp contrast enhancement. In some cases injection of the contrast media can be even excluded. Valuable information on local composition in the chosen region of interest (ROI) can be received with use of focusing polycapillary optics. The focused

* tour@mail1.lebedev.ru, phone:+7 095 132-62-68

X-ray and Neutron Capillary Optics II, edited by Muradin A. Kumakhov, Proc. of SPIE Vol. 5943 (SPIE, Bellingham, WA, 2005) · 0277-786X/05/$15 · doi: 10.1117/12.638003

X-ray beam can be itself an instrument for radiation treatment of biological tissue. In combination, it offers a unique opportunity of non-destructive visualization and procession of biological samples.

2. THE X-RAY MICROSCOPE PROJECTION AND MEASURING SCHEMES

Scheme of the X-ray microscope is shown in Fig. 1.

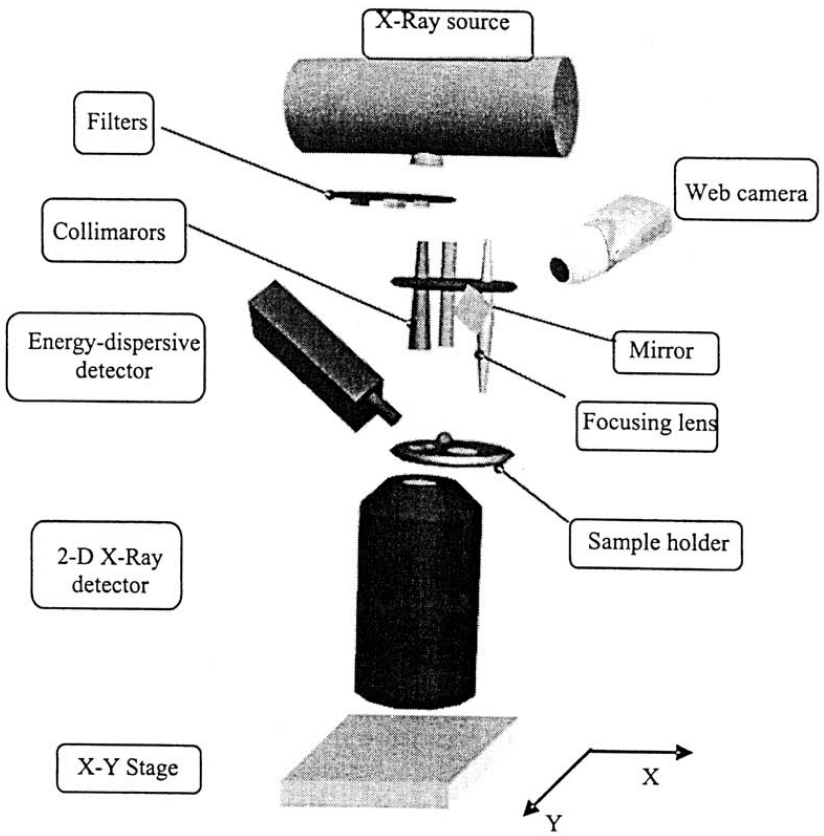

Fig. 1. Schematic diagram of the X-ray optical microscope

The radiation source is an air-cooled 50-W X-ray tube with a Cu or Mo anodes. Radiation with an energy <4 keV is partially filtered due to its attenuation in air. A ring-mount with four radiation disc filters and the Pb beam stopper are positioned in front of the X-ray tube window. The spectrum of X rays incident on the sample is typically modified by using an Al-, Ni-, and Cu foils. Filters provide an attenuation of the hard portion of the spectrum with an energy exceeding the *K*- edge of the photo absorption jump.

An X-ray beam is finally formed by a polycapillary lens or collimator tube with a diaphragm, which are installed in a ring-mount. The half-lens forms a quasiparallel beam with an angle divergence equal $\approx 2\theta_c$, where θ_c – a critical angle of the total external reflection for lens glass. An effective beam diameter coming out of the half-lens is 3-6 mm depending on the X-ray tube anode material and voltage applied to the tube. The half-lens serves also for filtration of hard part of the X-ray spectrum. The filtered and confined beam is passing through the sample positioned in a ring cassette serving as a sample holder. Up to 6 samples can be loaded for investigation.

The two-dimensional distribution of the radiation flux density is registered by an FDI camera (Photonic Science). The basic detector element is a CCD array with 1300 x 1030 photosensitive cells, a fiber-optic cable of variable cross section, and a scintillator layer deposited on the cable end. A Gd oxysulfide polycrystal with a surface density of 10 mg/cm^2 is

used as the scintillator. A two-stage cooling system based on Peltier elements reduces the temperature of the array by 40° as compared to the environment. Recording 16 exposures/s in a dynamic range of 10 bit is ensured at an interrogation rate f = 20 MHz. All of the results presented in this work were obtained at f = 10 MHz. In this case, a dynamic range of ~12 bits is attained. The diameter of the detector entrance window is 19 mm, and the effective working area of the detector is a rectangle with dimensions of 8.7 x 6.9 mm^2. The 0.25-mm-thick protective membrane is made of polished Be.

For preliminary sample examination in the optical range are used a mirror, high-resolution web camera, and light source (Fig. 2). The mirror is positioned on the ring–mount with lenses and collimator.

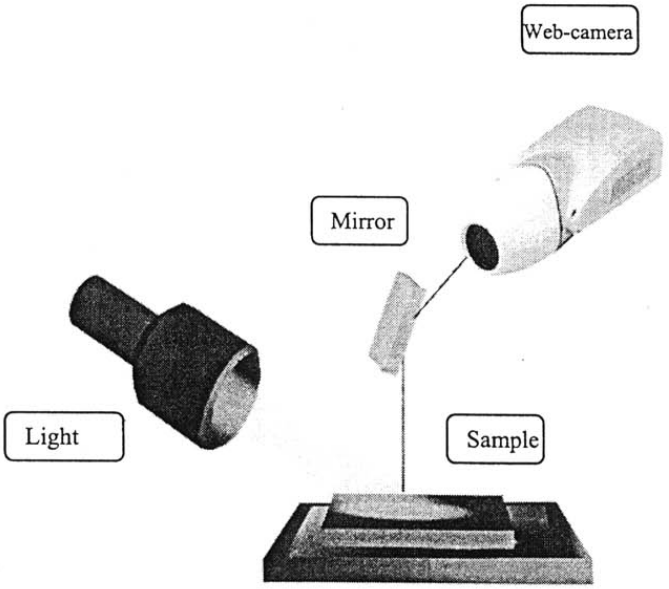

Fig. 2. Optical microscopy scheme

All the ring-mounts and sample holder are driven by the stepping motors connected to controllers.

3. BASIC OPERATION MODES

The microscope provides four basic operation modes: X-ray microscopy; optical microscopy; local X-ray fluorescence analysis and beam treatment by focused radiation.
The computer interface is used for controlling all moveable parts, data acquisition and data procession. Images and graphic materials are presented on the PC monitor. In beam treatment mode, according to calculations based on lens transmittance and focus size measurements, the dose rate up to 10 Gy is achieved for effective X-ray quanta energies ~ 10 keV. As X-ray fluorescence spectra are registered in air. Therefore, chemical elements with atomic number Z>12 can be determined. In both mentioned modes the same focusing lens is used providing focus size 150 μm.

4. CONTRAST ENHANCEMENT BY PROJECTION SUBTRACTION

In order to explain the features of the perception of the contrast of the image obtained as the difference of two projections, let us emphasize the chief differences between the images recorded in the analog and digital forms and some features of perceiving images in the visible range. Analyzing the contrast, we assume that the relative statistical fluctuations over the selected image element can be neglected compared to the relative change in the signal level quantized in the form of brightness gradations. As a rule, the contrast of an individual detail C_d of an image and the contrast over the entire image field C are analyzed.[9-13] When analog methods for recording the primary radiation image

are used, the following relations are most frequently used to numerically characterize C_d and C:

$$C_d = |\Delta I|/I, \quad (1)$$
$$C = (I_{max} - I_{min})/I_{max}, \quad (2),$$

where ΔI is a small increment of the analog signal of the photodetector created by this detail with respect to the level of the background signal I surrounding the detail. If $I \propto L$, where L is, for example, the screen glow brightness or the film blackening density, relations (1) and (2) also characterize the optical image of the illuminated object. In practice, when displaying the primary radiation image on a monitor screen, it is necessary to take into account the Weber–Fechner law[14] and perform a nonlinear conversion of the radiation signal. Therefore, the radiation and optical images usually have different contrast characteristics. As a measure of the quality of a radiation image, relation (2) becomes meaningless during digital recording. In fact, since, before displaying a digital image on a screen, it is possible to determine the I_{min} value using a program and subtract it from the elements of the data matrix, according to (2), any digital image after this procedure can formally have the maximum contrast value $C = 1$.

Under favorable visualization conditions (the image brightness is ~100 cd/m^2 and the angular size of the detail is no less than 0.3°, the minimum visually discerned contrast value is $C_{min} \approx 0.02$.[11] The range of the brightness ratio within which the eye can almost uniformly distinguish the contrast gradations produced by image details does not exceed $L_{max}/L_{min} = 35$.[15] According to the Weber–Fechner law, we have the following estimate of the number contrast gradations G_c within this range:

$$G_c = \frac{(\ln L_{max} - \ln L_{min})}{\ln(1 + C_{min})} \approx 180 \quad (3).$$

Hence, for discretely varying black-and-white gradations of the brightness L, it is sufficient to introduce an 8-bit brightness scale providing 256 gradations. It is precisely this scale on which modern graphics editors operating with black-and-white images are based.[16] Scales with wider ranges, such as 12 or 16 bits, are actually used for storing and numerically processing the data array.

In practice, due to the presence of external lighting, the impossibility of a long-duration eye adaptation, an angular dependence of the reflectivity, and other factors, the actually distinguishable range of gradations G_p is no larger than 6–7 bits. Therefore, in order to visually represent any projection containing digital data in the range of quantization levels of $G_e > G_p$, the projection must be transformed by dividing the data array elements by the ratio G_e/G_p. This leads to a loss of data. An alternative approach is to view the image in parts in a window containing the gradation range $(G_i, G_i + G_p)$, where G_i is the lower signal level selected by the observer.

During the digital image recording, the range of measured signal levels is usually much larger than the range of gradations perceived by the eye. For example, in computer tomography (CT), the range of registered gradations of the linear extinction factor in the form of Hounsfield units usually amounts to at least 10 bit, and the technically ensured range is >12 bit.[17] For this reason, the image is represented within a certain window of gradations selected automatically or by an operator. In this case, the image-field areas lying outside of the selected visualization window are represented by a black or white field. Thus, as applied to a digital image, it is expedient to speak about an optimal contrast at which the number of obtained contrast gradations corresponds to the number of visually perceived signal gradations over the entire image field. In this case, the main details of the object's internal structure must be preserved and the data array obtained must be suitable for calculating the parameters of the illuminated object.

When we change to the difference image obtained by subtracting the data array recorded at energies E_1 and E_2, expression (1) for the detail contrast is transformed and takes the form

$$C_d^s = |\Delta I_1 - \Delta I_2|/|I_1 - I_2|. \quad (4),$$

where I_1, I_2 – intensities measured at energies E_1, E_2 respectively. As it is demonstrated below the subtraction technique provides also stereoscopic effect that is very important for identification of image details.

Let us now assume for definitiveness that the element examined is a disk with a thickness Δx whose axis is parallel to the incident beam. This element lies in a layer of the substance whose composition and density differs from the element substance. The relative change in the signal produced by the element is small compared to the signal recorded upon passage of X rays through the object: $\Delta I_1 \ll I_1$ and $\Delta I_2 \ll I_2$. Let us assume that $E_1 < E_2$ and $I_1 \quad I_2$. Expanding the exponential function, which describes the extinction of monochromatic radiation in the substance, into a power series and rejecting the terms with a power exceeding one, after transformations, we obtain the following expression for the difference contrast:

$$C_d^s(E_1, E_2) = \frac{\Delta x|(\mu_1 - \gamma\mu_2)|}{|1-\gamma|}, \qquad (5)$$

where μ_1 and μ_2 are the linear coefficients of absorption for radiation with the energies E_1 and E_2, and $\gamma = I_2/I_1$.

5. RESULTS OF THE MICROSCOPE TESTING.

Major results of the X-ray microscope testing are presented in Figs 3-8

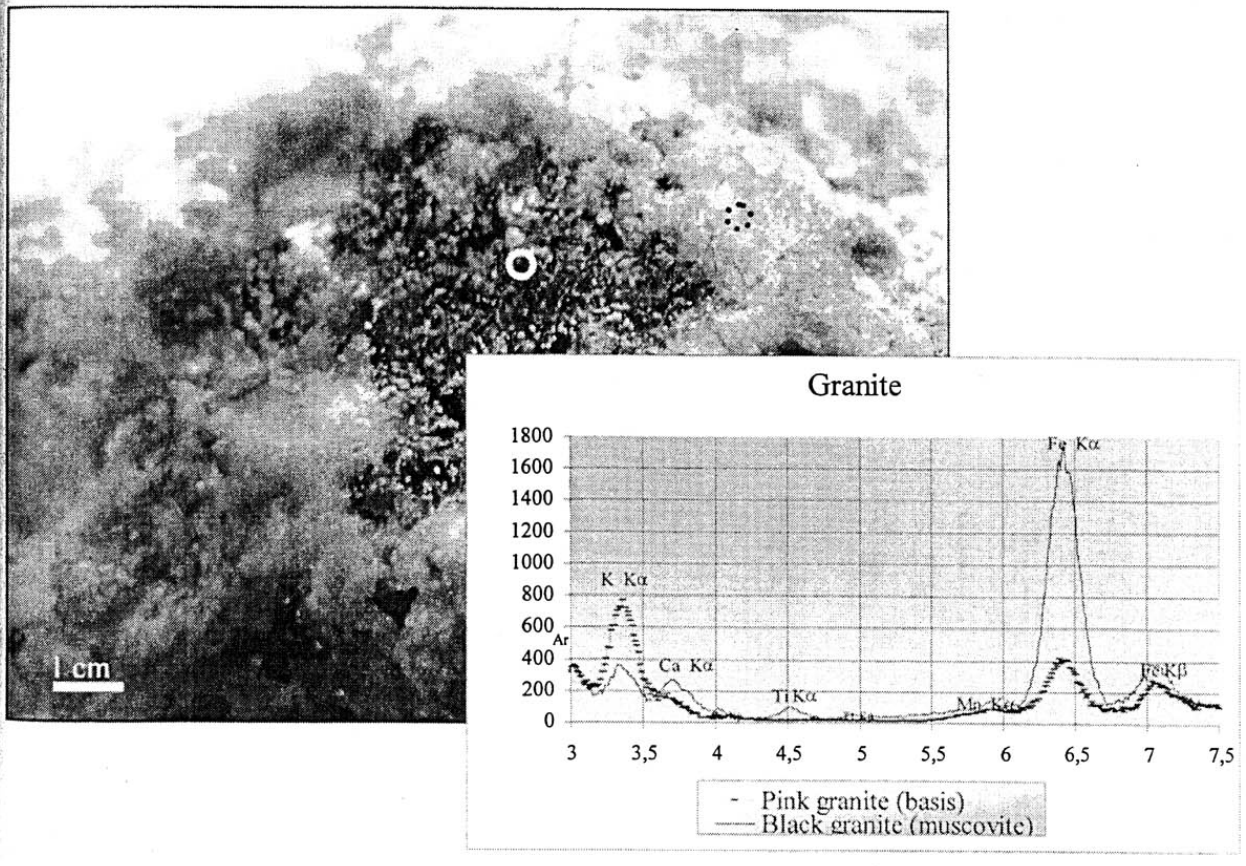

Fig. 3. Optical image of granite sample and X-ray fluorescence spectrum from the selected region of interest (solid circle – pink granite, dot circle – black granite)

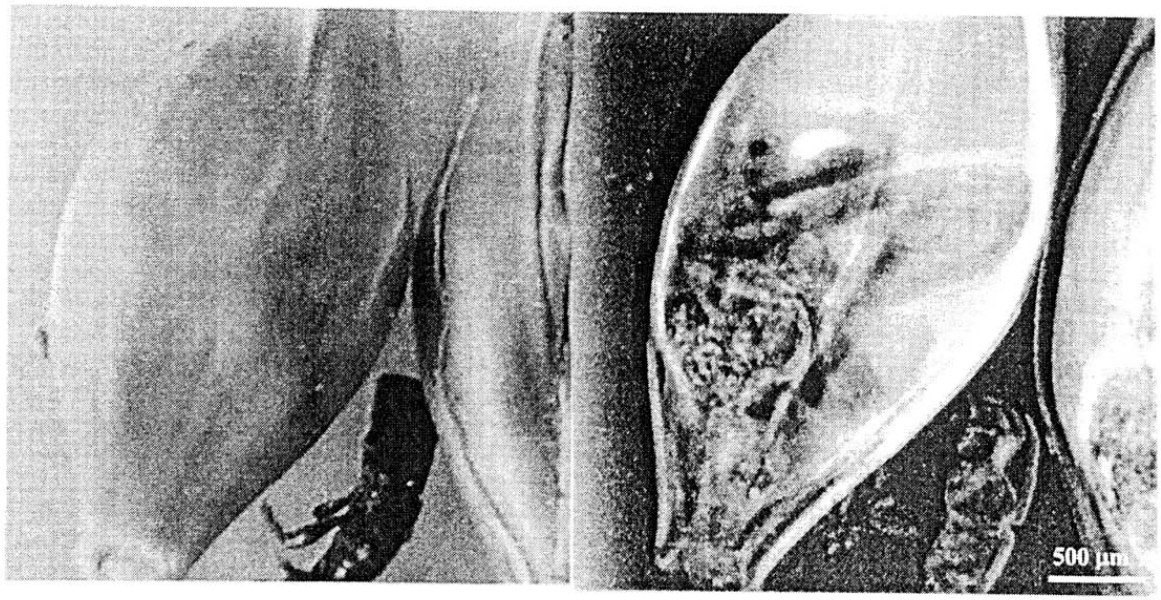

Fig. 4. Optical (left) and X-ray (right) images of the damaged barley seed with a bug

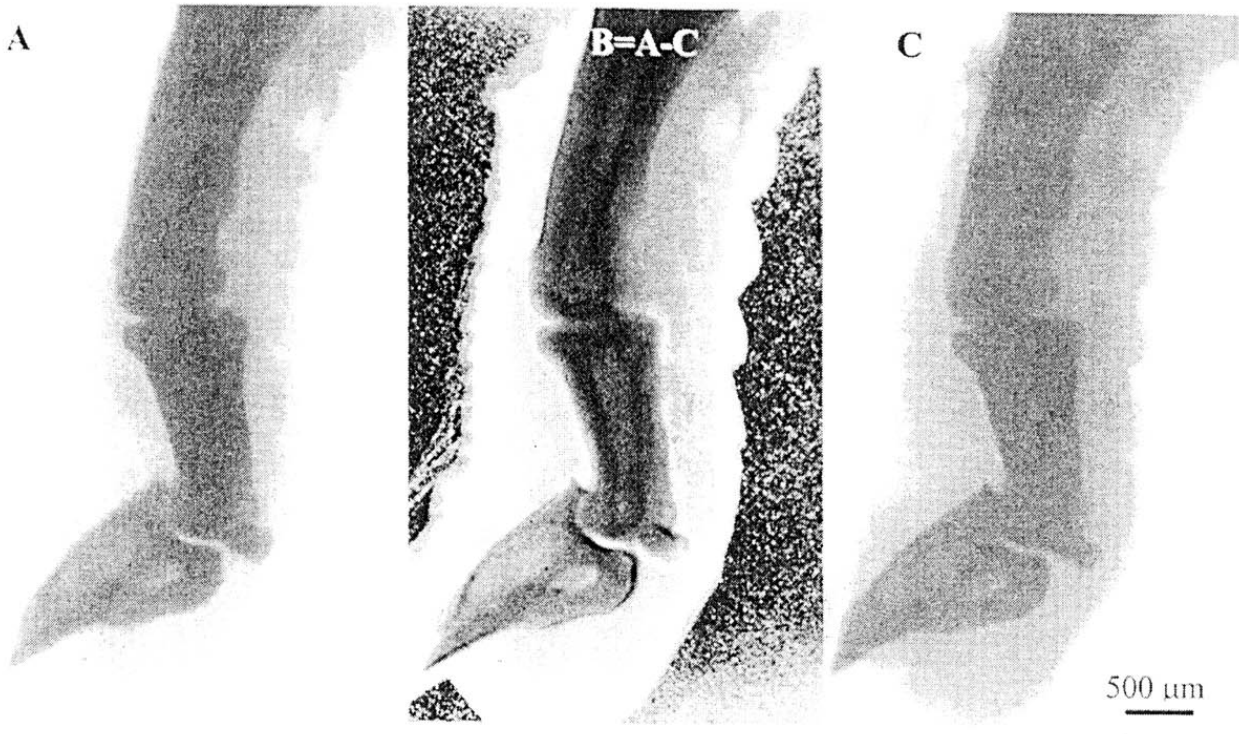

Fig. 5. The X-Ray image of rat's finger (in the centre – subtraction image, left and right images – standard X-ray projection)

A – 21kV; Ni – filter; B=A-C; C-16kV

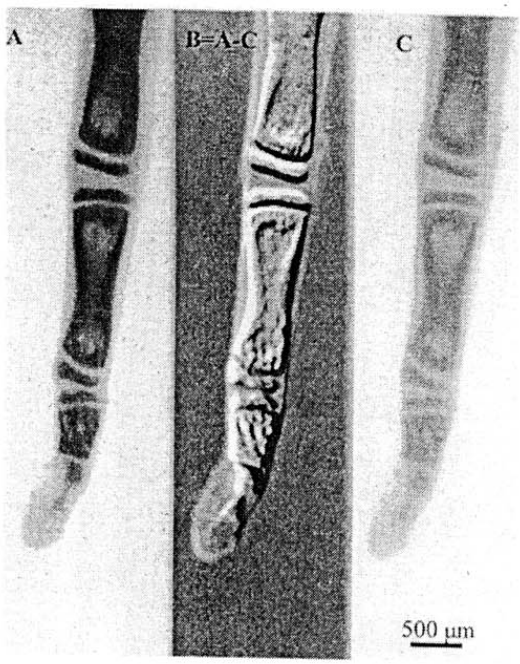

Fig. 6. The X-Ray image of rat's tail (in the centre – subtraction image) : A – 18kV; B=A-C; C-18kV, Ni filter;

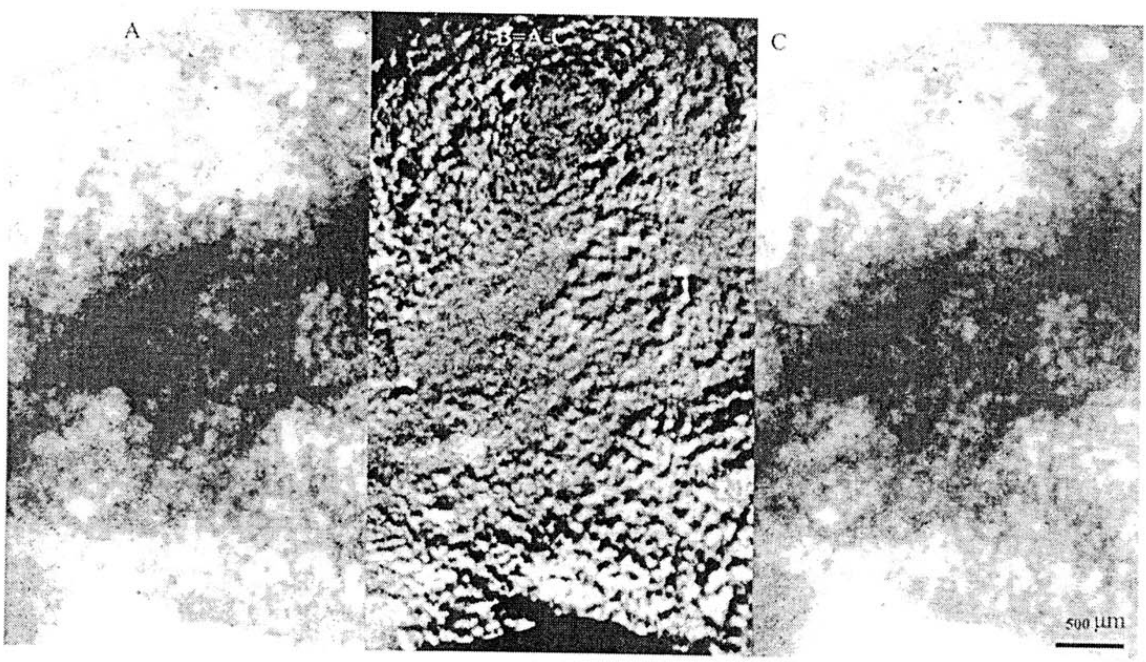

Fig. 7. The X-Ray image of frog's left lung : A – 19kV; Ni – filter; B=A-C; C-16kV

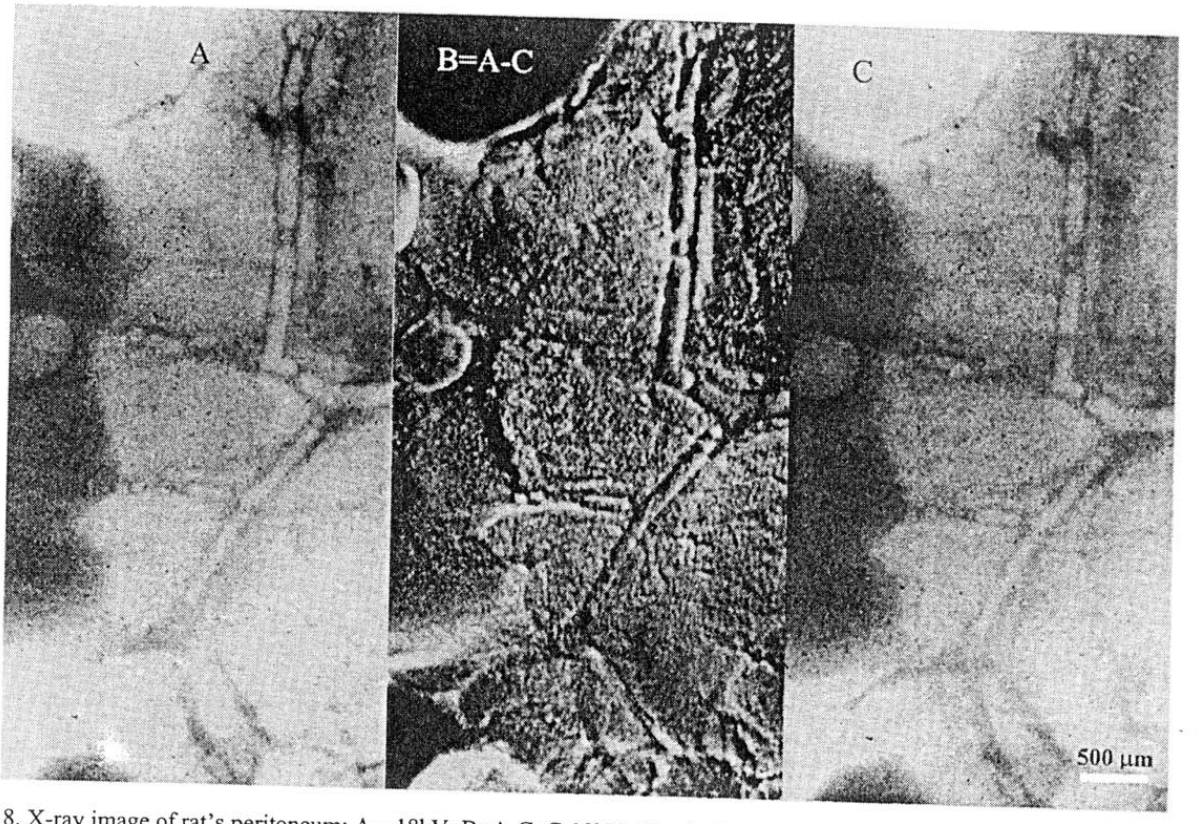

Fig. 8. X-ray image of rat's peritoneum: A – 18kV; B=A-C; C-18kV, 12-min frame acquisition interval, without contrast media.

REFERENCES

1. Lindenbraten, L.D. and Naumov, L.B., Medical Rontgenology, Moscow: Meditsyna, 1984.
2. Ishchenko, B.I., Bisenkov, L.N., and Tyurin, I.E., (Radiation Diagnostics for Thoracal Surgeons), St-Petersburg: DEAN, 2001, p. 346.
3. Handbook on Angiography, Rabkin, I.Kh., Ed., Moscow: Meditsyna, 1977, p. 288.
4. Sergeev, P.V., Sviridov, N.K., and Shimanovskii, N.L., X-ray Contrast Substances, Moscow: Meditsyna, 1980, p. 240.
5. Bykov, R.E., Kozlovskii, E.B., and Mazurov, A.I., Medical Introscopy Equipment, Leonov, B.I., Ed., Moscow: Meditsyna, 1989, pp. 103–143.
6. Kondratyev, V.I., Kulipanov, G.N., Kuzin, M.V., *et al.*, *Medical Applications of Synchrotron Radiation,* Ando, M. and Uyama, C., Eds., Tokyo: Springer, 1998, pp. 29–32.
7. Dill, T., Ventura, R., and Dix, W.-R., *et al, Medical Applications of Synchrotron Radiation*, Ando, M. and Uyama, C., Eds., Tokyo: Springer, 1998, pp. 22–28.
8. Bessonov, E.G., Vinogradov, A.V., and Tur'yanskii, A.G., *Prib. Tekh. Eksp.*, 2002, no. 5, p. 142.
9. Rumyantsev, S.V., Shtan', A.S., and Gol'tsev, V.A., A Handbook of Nondestructive Testing, Moscow: Energoatomizdat, 1982.
10. Electronics, Moscow: Sov. Entsiklopediya, 1991.
11. Gurvich, A.M., Physical Foundations of Radiation Control and Diagnostics, Moscow: Energoatomizdat, 1989.
12. Blinov, N.N., Bykov, R.E., Leonov, B.I., *et al.*, in Medical Introscopy Equipment, Moscow: Meditsyna, 1989, pp. 6–48.
13. Halmshaw, R., *Research Techniques in NondestructiveTesting*, Sharpe, R.S., Ed., London: Academic, 1970.
14. Krasil'nikov, N.N., Theory of Transmission and Perception of Images, Moscow: Radio i Svyaz', 1986, p. 248.
15. *Bildgebende Systeme Fur Medizinishe Diagnostik,* Berlin: Siemens Aktiongesellschaft, 1980.

16. Taits, A.M. and Taits, A.A Adobe(r) Photoshop 5.5. Self-Taught, St. Petersburg: BKhV-Sankt-Peterburg, 2000, p. 544.
17. Somatom Sensation. Siemens Medical. Brochure.